



Environmentally conscience corrosion inhibitors for mild steel in corrosive hydrochloric acid solution by *Uncaria Cordata* extract: experimental and theoretical studies

Nor Affanizam Othman, Ab Malik Marwan Ali, Noor Syafiqah Samsi, Fatimah Salim, Dedikarni Panuh, Muhamad Kamil Yaakob, Zaidi Embong, Ahmad Shalabi Md Sauri, Nik Norziehana Che Isa & Nor Zakiah Nor Hashim

To cite this article: Nor Affanizam Othman, Ab Malik Marwan Ali, Noor Syafiqah Samsi, Fatimah Salim, Dedikarni Panuh, Muhamad Kamil Yaakob, Zaidi Embong, Ahmad Shalabi Md Sauri, Nik Norziehana Che Isa & Nor Zakiah Nor Hashim (2023): Environmentally conscience corrosion inhibitors for mild steel in corrosive hydrochloric acid solution by *Uncaria Cordata* extract: experimental and theoretical studies, Journal of Adhesion Science and Technology, DOI: [10.1080/01694243.2023.2196905](https://doi.org/10.1080/01694243.2023.2196905)

To link to this article: <https://doi.org/10.1080/01694243.2023.2196905>



Published online: 10 Apr 2023.



Submit your article to this journal [↗](#)




View related articles [↗](#)



View Crossmark data [↗](#)



Environmentally conscience corrosion inhibitors for mild steel in corrosive hydrochloric acid solution by *Uncaria Cordata* extract: experimental and theoretical studies

Nor Affanizam Othman^a, Ab Malik Marwan Ali^{a,b}, Noor Syafiqah Samsi^{a,b}, Fatimah Salim^{a,c}, Dedikarni Panuh^d, Muhamad Kamil Yaakob^a, Zaidi Embong^e, Ahmad Shalabi Md Sauri^f, Nik Norziehana Che Isa^g and Nor Zakiah Nor Hashim^g 

^aFaculty of Applied Sciences, Universiti Teknologi MARA, Shah Alam, Selangor, Malaysia^bInstitute of Science, Universiti Teknologi MARA, Shah Alam, Selangor, Malaysia; ^cAtta-ur-Rahman Institute for Natural Product Discovery (AuRIns), Bandar Puncak Alam, Selangor, Malaysia; ^dDepartment of Mechanical Engineering, Islamic University of Riau, Riau, Indonesia; ^eDepartment of Physics and Chemistry, Universiti Tun Hussein Onn Malaysia, Muar, Johor, Malaysia; ^fPETRONAS Research Sdn Bhd, Kawasan Institusi Bangi, Kajang, Selangor, Malaysia; ^gCentre of Foundation Studies, Universiti Teknologi MARA, Selangor, Malaysia

ABSTRACT

The *Uncaria Cordata* as corrosion inhibitors for mild steel (MS) in a 1.0M hydrochloric acid (HCl) solution. The EIS, polarization, and LPR measurements were used as experimental measurements to confirm the anti-corrosion performances of the *Uncaria Cordata* at room temperature. The corrosion inhibitors, even at a low dosage range, achieved inhibition efficiencies to a maximum of 97.0% for 400 ppm of *Uncaria Cordata*. Surface morphology via AFM and SEM/EDX was carried out to validate the presence of protected film and an optimum concentration of each extract above the metal's surface in the corrosive acidic solution. The ΔG°_{ads} value – 19.70 kJ/mol proved a spontaneous merge of physical and chemical adsorption by the extract compounds at the interface of MS and the HCl solution. DFT was governed to accommodate the elevated inhibition efficiency upshot obtained by the electrochemical tests and recommend a synergy mechanism for most of the adsorbed active compounds in *Uncaria Cordata* inhibitors with the MS surface. Monte Carlo simulation indicates three active compounds, namely **1**, **2**, and **8**, found to have parallel adsorption on MS. This encourages the highest surface coverage and shields the MS surface from the intrusion of corrosive agents.

ARTICLE HISTORY



Received 1 February 2023
Revised 22 March 2023
Accepted 25 March 2023

KEYWORDS

Uncaria Cordata; corrosion inhibitor; mild steel; DFT; Monte Carlo

1. Introduction

In battling corrosion, the film-forming inhibitors are apprehended to be an exceptional method to protect mild steel (MS) in an acidic medium [1]. By standard

CONTACT Nor Zakiah Nor Hashim  norzakiah@uitm.edu.my  Centre of Foundation Studies, Universiti Teknologi MARA, Cawangan Selangor, Kampus Dengkil, Dengkil 43800, Selangor, Malaysia.

© 2023 Informa UK Limited, trading as Taylor & Francis Group

definition, a corrosion inhibitor is categorized as a chemical material amplified in an optimal concentration to a corrosive solution that reduces the metal corrosion rate without affecting its mechanical resistance. Corrosion inhibitors must be dependable and reliable in slowing down the rate of metal deterioration even tested under factors such as various concentrations, film stability, and durability as well as different pH's [2,3]. Furthermore, the tested compounds should be competent in combating metal corrosion even in a low concentration, easily available, and less harmful to the living organism [4].

As a movement to advocate this concept, the practice of plant extract serving the “green” chemistry concept is tremendously suggested [5,6]. The apparent reason for plant extracts to be categorized as green and feasible are due to the element/natural and its abundance of biological abilities to combat metal corrosion immediately upon exposure to the corrosive solution under assessment [7]. For leafy plants, the leaf part has the highest popularity among researchers to be selected as an excellent corrosion inhibitor due to its richness of active components (phytochemicals) [8], which are extracted *via* selected suitable solvents to extract the target bioactive compounds [9]. Other extracted parts of the plant, such as seed, peel, stem, flower, and so forth, also have shown high inhibition efficiencies [3].

The utilization of mild steel (MS) is sweepingly employed in countless industries, specifically with a corrosive acidic solution. This includes but is not limited to petrochemical operations, crude oil enrichment, and oil retrieval in the oil and gas division. The processes that are involved in these stages of operations, for instance, acid pickling, industrial cleaning, and acid descaling, require periodical maintenance to ensure the high quality, productiveness, and yield of the desired products [10,11]. Generally, the strong acid employed for this process is phosphoric acid, hydrochloric acid, or sulfuric acid on account of the robust corrosiveness in dissolving scales besides unique chemical properties [11,12]. Customarily, in upstream production facilities, especially deep gas wells, hydrochloric acid is inserted to activate the well by upgrading formation permeability [13].

Next, genus *Uncaria* (Rubiaceae) plants exist in 34 species dispersed mostly in tropical and subtropical Asia, Africa, as well as tropical America [14]. Amongst the 14 species of *Uncaria* found in Peninsular Malaysia, the *Uncaria cordata* var. *ferruginea* is one of the most common. Previous reported phytochemical studies on the stem and leaves extract of the undergoing study for *Uncaria Cordata* produced more than a few active compounds. *Uncaria Cordata* includes quercetin, kaempferol, scopoletin, taxifolin, 3,4-dihydroxybenzoic acid, 2-hydroxybenzoic acid, 2,4-dihydroxybenzoic acid, loganin, and β -sitosterol [15]. Additionally, it was also shown that *Uncaria gambir* extract remarkably reduces the corrosion rate of MS in an acidic solution [16], which encourages the authors to test *Uncaria cordata* stem and leaves extract as an environmentally friendly corrosion inhibitor against the corrosion of MS in 1.0 M HCl experimentally as well as theoretically. The corrosion inhibition analysis techniques involved are Electrochemical Impedance Spectroscopy (EIS), Polarization, and Linear Polarization (LPR) Measurements. Next, surface morphological studies by Scanning Electron Microscopy (SEM) and Atomic Force Microscopy (AFM) were both implemented to compare the surface of MS in the uninhibited versus inhibited

solution. Furthermore, the theoretical assessment using quantum chemical calculations is imperative in strengthening the theory of adsorption mechanism for the studied *Uncaria Cordata* in protecting the outer of MS from corrosion in the acidic environment. The corrosion inhibition efficiencies are highly reliant on the electronic properties and physicochemical of the *Uncaria Cordata*, which may rise to produce high proficiencies film to insulate the MS surface from the invasion of corrosive species in the solution even at an extended period. Furthermore, Monte Carlo simulation discovered the active compounds in the corrosive solution adsorbed on the surface of MS that promote maximum surface coverage and prove theoretically the arrangement of a non-penetrate film by the extract of *Uncaria Cordata* molecules from the intrusion of corrosive agents at the metal-solution interface.

2. Methodology

2.1. Extraction of *Uncaria Cordata* species

2.2. Plant matter

The attainment of stems and leaves of *Uncaria cordata* var. *ferruginea* was from Hutan Simpan Bangi, Selangor, Malaysia ($101^{\circ} 45' 969''$, $02^{\circ} 55' 016''$). The corresponding voucher specimens of HTBP 1336, HTBP 4318, and HTBP 1336 were amassed at Taman Botani Putrajaya, Malaysia [15].

2.3. Extraction of raw extracts

The stems and leaves of the plants were independently incised in minor portions, left to dry in an open environment, crushed into lightweight powder, and weighed. The finely powdered parts of *Uncaria Cordata* var. *ferruginea* were exhaustively extracted for 72 h using methanol at ambient temperature. The extracts' solvent was vaporized through a compressed pressure, and the extract's mass was filed [15]. Figure 1 illustrates the chemical structures for the main components in the leaves and stem of *Uncaria Cordata* as discovered by one of the authors [15].

2.4. Samples

The MS (Q-Panel) specimen as a working electrode with a chemical composition of C: 0.25 – 0.290%, Cu: 0.20%, Fe: 98.0%, Mn: 1.03%, P: 0.040%, Si: 0.280%, S: 0.050% was assembled by the following practice: the electrodes were constructed by implanting the MS panel in an epoxy resin, disclosing a geometrical plane area of 0.049 cm^2 of the MS panel to the caustic solution. The exposed MS surface was abraded utilizing dissimilar grades of silicon carbide papers (600, 1000, and 1200) and afterward polished using $1 \mu\text{m}$ of Diamond Polish (DP) Spray. The sample was washed a few times using deionized water, removed from grease with ethanol, and dried.

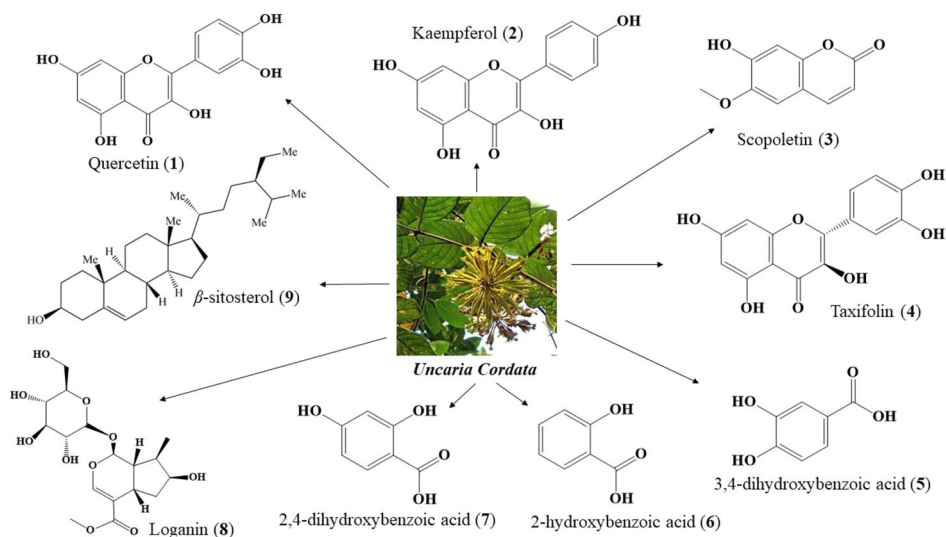


Figure 1. Chemical structures for the main components in the leaves and stem of *Uncaria Cordata* var. *ferruginea*.

2.5. Test solution

The electrochemical method was completed using 1.0 M HCl solution in the inhibited, along with an uninhibited solution of the deliberated *Uncaria's Cordata* in the concentration limitation between 100 ppm to 400 ppm. The aggressive medium was formulated using HCl (37% w/w) and diluted in deionized water.

2.6. Electrochemical impedance spectroscopy (EIS) measurement

Impedance evaluations were executed following a half-hour of fully submerging the MS as a working electrode in a uniform solution at a constant state open circuit potential (E_{ocp}) at 25 °C. The assessment was fulfilled in an average three-electrode cell with a silver-silver chloride reference electrode (Ag|AgCl|Cl⁻) and a platinum (Pt) as a counter electrode. The alternating current frequency covers the range of 100 kHz to 0.1 Hz with an amplitude of 0.01 V peak-to-peak. The investigation was implemented using a workstation linked to PGSTAT302N. The polarization resistance, R_p , and solution resistance, R_s , values were extrapolated from semicircles in the Nyquist plots.

2.7. Polarization and linear polarization measurements

The polarization measurements were conducted promptly after EIS measurements with an identical working electrode versus the reference electrode (Ag|AgCl|Cl⁻) in the absence of extra surface preparation. The applied potentials were swept using a scan rate at 1 mVs⁻¹ from the corrosion potential (E_{corr}), first oriented towards the cathodic region, succeeded by the anodic region. Inhibition efficiencies ($\eta_{pol}\%$) were deliberated by implementing the resulting equation [17]:

$$\eta_{pol}(\%) = \frac{i_{corr} - i'_{corr}}{i_{corr}} \times 100 \quad (1)$$

where i_{corr} and i'_{corr} specifies corrosion current densities in uninhibited and inhibited solutions in sequence.

Subsequently, polarization resistance (R_p) values were quantified by the equation of potential over the current's slope as in [18]:

$$R_p = A \frac{\Delta E}{\Delta i} \quad (2)$$

The R_p values are implemented to resolve the inhibition efficiencies, in which A is attributed to the working electrode's surface area, while ΔE and Δi are the changes in the potential and current, accordingly.

$$\eta_{Rp}(\%) = \frac{R_{p(inh)} - R_p}{R_{p(inh)}} \times 100 \quad (3)$$

where in $R_{p(inh)}$ and R_p are inhibited and uninhibited polarization resistance respectively [19].

The corrosion rates (CR) were determined in millimeters in a year based on the equation [20]:

$$\text{Corrosion rate} \left(\frac{mm}{yr} \right) = 0.00327 \frac{i_{corr} \left(\frac{\mu A}{cm^2} \right) \times EW}{\text{density} \left(\frac{g}{cm^3} \right)} \quad (4)$$

in which 0.00327 is a fixed value for dimensions with time conversion element, whereas EW is the equivalent weight for MS in grams.

2.8. Scanning electronic microscopy (SEM)/energy Dispersive X-Ray Spectroscopy (EDX)

The surface morphology of MS using SEM was practiced conforming to the efficiencies of the inhibitors under investigation to conserve the external condition of the metal, even when it has been exposed to the corrosive medium for an extended time frame. The effectiveness of the corrosion inhibitor has been deliberated by correlating the variation on the MS surface at a microscopic standard in the inhibited medium. The specimens of MS were prepared in the dimension of 1 cm^2 before being fully immersed for the duration of 24 h in 1.0 M HCl solution (blank solution) and inhibited solution containing 400 ppm inhibitors. The MS samples were drawn out from the acidic solution, brushed, cleaned with absolute ethanol, and dried. The MS substrate was sputter-coated with gold (Au) and then examined with SEM images at a magnification of 4300X and voltage of 10 kV combined with an EDX component. In the EDX analysis, the acceleration voltage employed in the current study was 15 kV. These analyses were achieved in Phenom-World's proX desktop SEM.

2.9. Atomic force microscopy (AFM)

AFM is a powerful surface-imaging tool for studying the surface at sub-micro-and nanoscales levels, as well as able to assess the effect of the thin film formation on the metal's surface [21,22]. In this study, the MS samples were prepared as in the SEM technique before being fully submerged in a blank solution of 1.0M HCl solution and in the acidic solution with the presence of 400 ppm corrosion inhibitors. After a twenty-four-hour period of being completely immersed in that solution, samples were pulled out then lightly brushed, cleaned with absolute ethanol, followed by deionized water to remove any remaining impurities, and air-dried. The specimens were examined using AFM to achieve 2D and 3D images of the size and height of the MS surface by quantifying the forces amidst an acute tip and the deliberated samples.

2.10. DFT calculations

Density Functional Theory (DFT) was conducted in Materials Studio 2016 by utilizing the DMol3 module available in the software to forecast the electronic, molecular, and adsorption attributions of the major components identified in *Uncaria Cordata* at the molecular level. The geometry of the compounds was first optimized by utilizing the hybrid functional of Becke three-parameter Lee, Yang, and Parr (B3LYP) combined with double Numerical plus polarization (DNP) basis set. The hybrid functional B3LYP is commonly used for calculating electronic structure and organic molecule properties [23–25].

2.11. Monte Carlo simulation

The adsorption attributes of active components were analyzed by conducting a Monte Carlo simulation to study their adsorption characteristics. Low-energy configuration and adsorption energies of the extract components on the densely packed Fe(110) surface [26–28] in a vacuum, as well as in a hydrochloric acid solution, were determined through the Adsorption Locator module in Materials Studio 2016 [29–31].

The Fe(110) surface with periodic boundary conditions was constructed using pre-optimized bulk metal structures from the software itself and comprised 6 layers of Fe atoms in a 15×15 unit cell. A 40 Å vacuum layer was added to the model to provide sufficient distance between the Fe surface and the next layer beyond the vacuum. Figure 2 illustrates the Fe(110) vacuum slab model with dimensions of $39.718 \text{ \AA} \times 39.718 \text{ \AA} \times 50.134 \text{ \AA}$ used for the simulation study. The chosen size parameters were grossly overestimated to prevent any non-bond interaction arising from the boundary conditions. A fine convergence level was selected for the simulation, which employs 5 temperature cycles with 50,000 steps for the respective temperature cycle in the simulated annealing run.

3. Result & discussion

3.1. Electrochemical impedance Spectroscopy measurement (EIS)

The EIS is a verified approach for rapidly evaluating the adsorbed corrosion inhibitor's efficiencies in forming a protective film at the metal-to-aqueous solution interface [32].

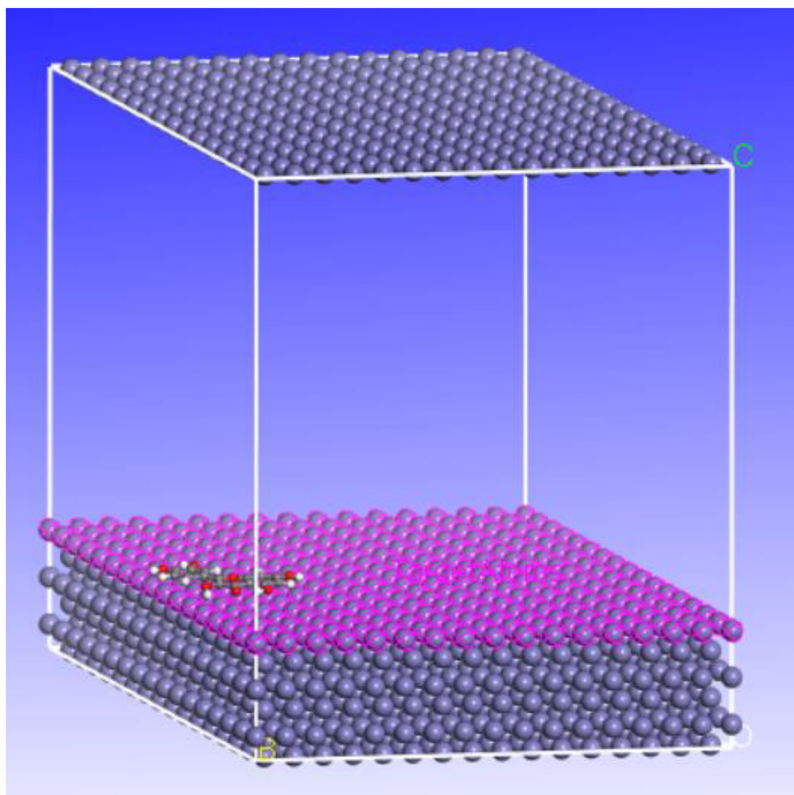


Figure 2. Fe(110) vacuum slab model for Monte Carlo simulation with an inhibitor molecule for comparative purposes.

The concentration ranges selected for this experiment are between 100 and 400 ppm. The minimum values of inhibitor's concentrations represent the lower inhibition efficiencies for the inhibitors, whereas the higher ranges concentrations depict the anti-corrosion accomplishment had achieved maximum efficiencies and remained constant even further increase in the insertion of inhibitors to the 1.0 M HCl solution [33].

Figure 3 illustrates the semicircle Nyquist plots for the working electrodes embedded with MS in 1.0 M HCl solution inclusive and excluding *Uncaria Cordata* as corrosion inhibitors. From the figure, the changes to the impedance action are observed following the incorporation of distinct ranges of inhibitors to the MS in the acidic solution of 1.0 M HCl at 25 °C in comparison with uninhibited solutions. The EIS measurement starts by analyzing the 1.0 M HCl solution (blank solution), which serves as a reference solution against the inhibited solutions. The gradual increase of corrosion inhibitor assimilating the 1.0 M HCl solution affects the size of the Nyquist semi-circle compared to uninhibited 1.0 M HCl. The reinforced semicircle diameter with the increase of inhibitor concentration stipulates the resilient insulating film on the MS surface. Next, the Nyquist semi-circle exhibited a single capacitive loop in the blank solution, as well as most of the inhibited solutions highly advocating that disintegration of MS, is a charge-transfer controlled reaction [34]. The entire EIS spectra are semicircles and well suited to the Randles circuit Figure 4, where the elements

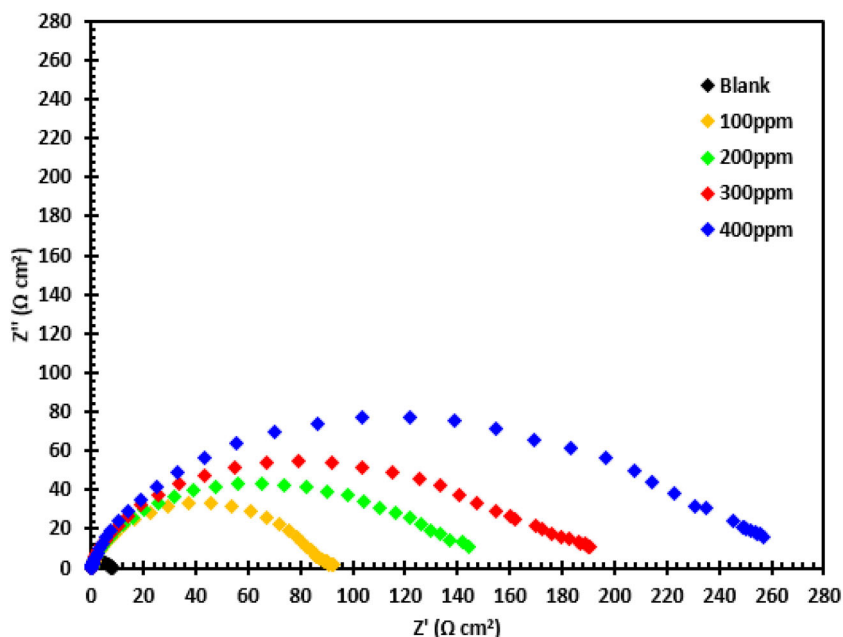


Figure 3. Nyquist plots for MS in 1.0 M HCl inclusive of various concentrations of *Uncaria Cordata* inhibitor and excluding of inhibitor at 25 °C.

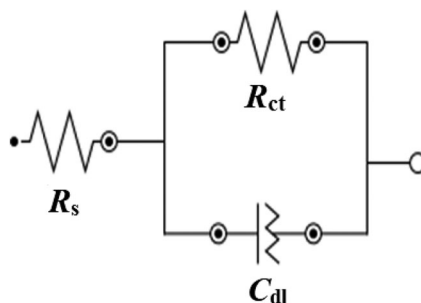


Figure 4. The implemented equivalent circuit in fitting impedance spectra for MS in 1.0 M HCl inclusive of several concentrations of *Uncaria Cordata* inhibitor and excluding of inhibitor at 25 °C.

involved are solution resistance (R_s), charge-transfer resistance (R_{ct}), and double-layer capacitance (C_{dl}). The related resistance values and impedance variables are tabulated in Table 1. Afterward, the C_{dl} was established by applying the equation [35,36]:

$$C_{dl} = \frac{1}{2\pi f_{max} R_{ct}} \quad (4)$$

in which f_{max} is the maximal frequency, whereupon the maximum imaginary constituent of the Nyquist plot. The R_{ct} exhibits an inverse connection to i_{corr} hence the inhibition efficiency $\eta_{EIS}(\%)$ is evaluated by quantifying the corresponding equation [37,38]:

Table 1. Impedance parameter evaluation for dissolution of MS in 1.0 M HCl inclusive of several concentrations of *Uncaria cordata* inhibitor and excluding of inhibitor at 25 °C.

Compound	Inhibitor Concentration (ppm)	R_s (Ω cm ²)	R_{ct} (Ω cm ²)	C_{dl} (μ F cm ⁻²)	n	η_{EIS} (%)
Blank	0	5.24	7.40	67.96	0.87	0.00
<i>Uncaria Cordata</i>	100	11.22	87.61	78.16	0.91	91.60
	200	39.47	143.86	53.47	0.89	94.90
	300	21.55	170.10	32.04	0.87	95.69
	400	23.82	247.75	28.57	0.92	97.00

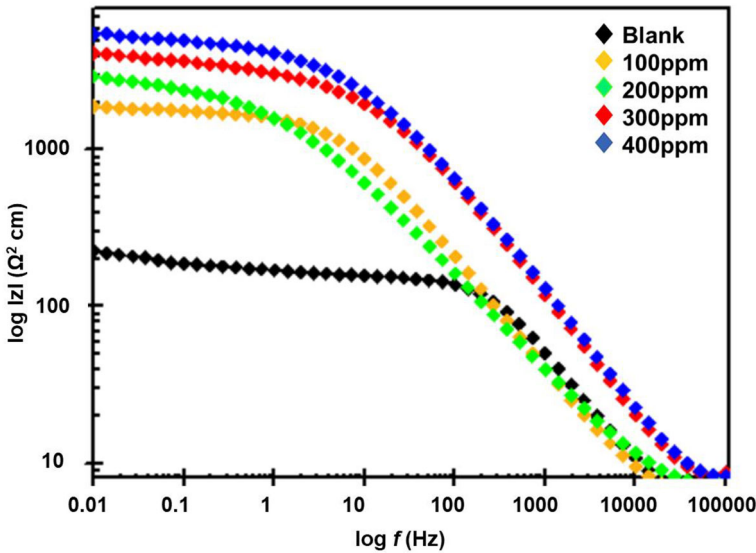


Figure 5. Bode plots for MS in 1.0 M HCl inclusive of various concentrations of *Uncaria Cordata* inhibitor and excluding of inhibitor at 25 °C.

$$\eta_{EIS}(\%) = \left(\frac{R_{ct(inh)} - R_{ct}}{R_{ct(inh)}} \right) \times 100 \quad (5)$$

where $R_{ct(inh)}$ and R_{ct} are assigned as inhibited and uninhibited charge transfer resistance.

By referring to [Table 1](#), higher amounts of corrosion inhibitors in the 1.0 M HCl enhanced the R_{ct} values, and in contrast, the C_{dl} values decline. It indicates the adsorption of active components in the *Uncaria Cordata* extract on the MS surface which later developed into a stable insulative film from the ingress of electrolytes that are in contact with the metal-solution interface. At the maximum concentration of 400 ppm, the corrosion resistance of this organic inhibitor film may achieve as high as 97.0% of inhibition efficiency. Thus, the trend in EIS outcome is found to have a reasonable correlation with polarization and linear polarization measurement.

The resistive and capacitive behavior for the highest corrosion inhibition achieved by *Uncaria Cordata*, as found in [Figure 3](#), may be further considered using Bode plots [Figure 5](#) and phase angles [Figure 6](#). The advantage of Bode plots is that it produces visible details on the relation of real impedance with the frequency as well as

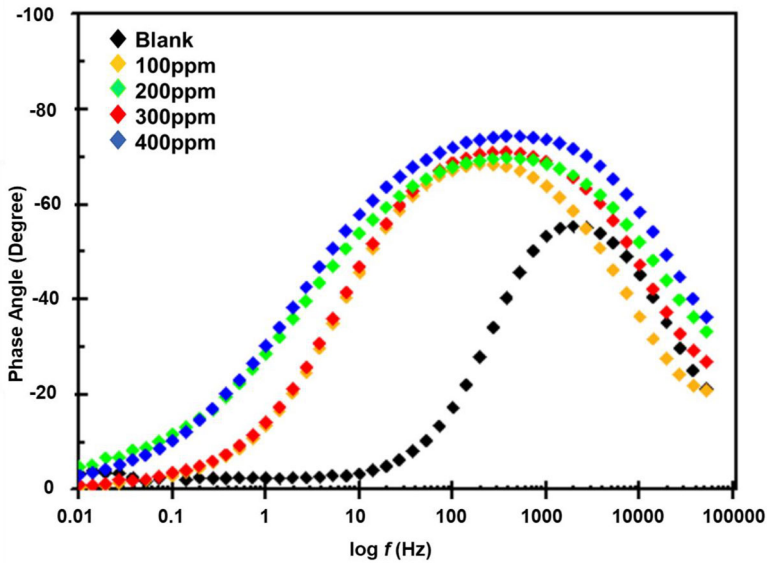


Figure 6. Phase angle for MS in 1.0M HCl inclusive of various concentrations of *Uncaria Cordata* inhibitor, and excluding of inhibitor at 25°C.

the phase angle in [Figure 6](#). Thus, at the area of low frequency for the bode modulus plot, real impedance values are heightened with the increased amount of *Uncaria Cordata* extract until it accomplished an optimum concentration of the inhibitor, which suggests the creation of a shielding film on the MS surface is in the most stable form [39].

In general, the capacitor that behaves ideally is defined if the slope values for Bode plots achieved -1 , as well as for phase angle attained -90° [40,41]. The relationship amongst $\log |Z|$ in contradiction of $\log f$ in the region of the mid of frequencies in the Bode plot displays slopes which are approaching -1 [Figure 5](#) and the phase angle hitting the highest at -74° [Figure 6](#). The sharp slope and a higher degree of phase angle for the 1.0 M HCl comprising of an elevated amount of *Uncaria Cordata* extract as opposed to the uninhibited solution proposing improvement and high conformity of the insulating layer of film on the MS surface.

3.2. Polarization and linear polarization resistance measurements

[Figure 7](#) indicates Tafel plots obtained for MS in the 1.0M HCl and inhibited solution consisting of *Uncaria Cordata* extract in distinct concentrations. As shown in [Table 2](#), the attained corrosion parameters for inhibitors include corrosion current densities (i_{corr}), corrosion potential (E_{corr}), anodic and cathodic slopes (β_a and β_c), polarization resistance (R_p), surface coverage (θ), and percentage of inhibition efficiencies ($\eta_{Pol}\%$) are tabulated. The parameters obtained distinctly demonstrate i_{corr} values are minimized with the increased amount of inhibitor in the corrosive 1.0M HCl. The established values for i_{corr} in distinction to the lowest concentration of inhibitors up to the highest concentration are decreased from 101.43 to 40.77

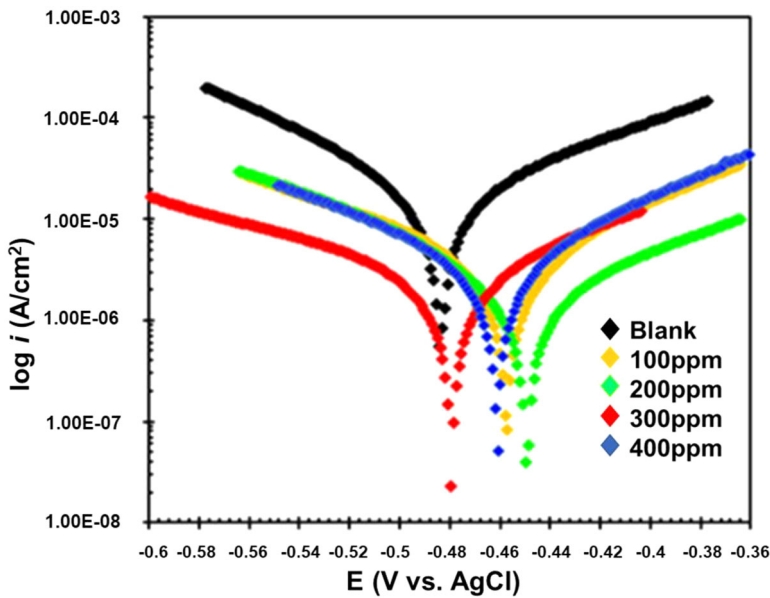


Figure 7. Tafel plot for MS in 1.0M HCl inclusive of various concentrations of *Uncaria Cordata* inhibitor and excluding of inhibitor at 25 °C.

Table 2. Corrosion parameter evaluation by polarization measurement for the dissolution of MS in 1.0M HCl inclusive of several concentrations of *Uncaria cordata* inhibitor, and excluding of inhibitor at 25 °C.

Compound	Inhibitor Concentration (ppm)	i_{corr} ($\mu\text{A cm}^{-2}$)	$-E_{corr}$ (mV)	β_a (mV dec^{-1})	β_c (mV dec^{-1})	CR (mm/yr)	η_{Pol} (%)	θ
Blank	0	432.53	483.74	155.03	131.46	21.19	0.0	0.00
<i>Uncaria Cordata</i>	100	101.43	457.30	99.78	95.56	4.02	77.0	0.77
	200	73.01	449.25	86.43	110.35	2.59	83.1	0.83
	300	55.81	459.38	78.74	98.71	2.23	87.1	0.87
	400	40.77	437.31	91.55	86.99	1.43	90.6	0.91

$\mu\text{A/cm}^2$, respectively. Next, the acquired verdict was signified with the reinforcement of η_{Pol} (%), which is simultaneous with the decrease of i_{corr} values [42,43]. Hence, it was found at 400 ppm solution containing inhibitors, the highest η_{Pol} (%) at 90.6% has been achieved for the *Uncaria Cordata* extract. The adsorbed inhibitors on the MS interface produce a protection film from the intrusion of ions from the electrolyte and are highly stable as shown in the highest concentration (400 ppm) of inhibitors [24].

The deterioration rates of MS are significantly reduced at the highest concentration of *Uncaria Cordata* extract contrary to the uninhibited solution, which stipulates the optimum adsorption of active components in the *Uncaria Cordata* on the exposed surface MS in the solution. Next, the 1.0 M HCl recommend corrosion of MS (anodic reaction) readily gives off iron (Fe) ions at the interface of MS metal/aqueous acidic solution and concurrently the hydrogen discharges (cathodic reaction) to the solution. Through the ideal amount of addition of inhibitors to the corrosive solution, it may affect either one or both reactions stated above (anodic and cathodic reactions) [25].

Table 3. Corrosion parameter evaluation by linear polarization measurement for the dissolution of MS in 1.0 M HCl inclusive of several concentrations of *Uncaria cordata* inhibitor and excluding of inhibitor at 25 °C.

Compound	Inhibitor concentration (ppm)	$-E_{corr}$ (mV)	R_p ($\Omega \text{ cm}^2$)	η_{Rp} (%)	CR (mm/yr)
Blank	0	483.74	1.130	–	21.20
<i>Uncaria cordata</i>	100	457.30	9.897	89.0	4.02
	200	449.25	10.158	89.0	2.59
	300	459.38	10.499	89.2	2.23
	400	437.31	12.690	91.1	1.43

Furthermore, the Tafel plots disclose the inclusion of the inhibitor's incorporation at the range of 100 ppm until 400 ppm to the aqueous solution of 1.0 M HCl significantly affects both Tafel slope parameters, which signifies the slows down of corrosion kinetics, especially in the anodic and cathodic reaction. The alteration in β_a and β_c slope parameters directly correlates with the mechanism of the hindrance of active spots on the iron surface and the cathodic hydrogen evolution reaction [44]. A small change in the arrangement of Tafel's anodic and cathodic gradients with the increased incorporation of inhibitors in the solution indicates a constant in the growth mechanism of hydrogen for the cathodic polarization curves, therefore suggesting activation-controlled for the hydrogen evolution reaction [45,46].

Based on previous studies [47–49], the corrosion inhibitors are designated as anodic or cathodic inhibitors on condition that the difference in shifting of E_{corr} for inhibited and uninhibited is more than ± 85 mV [50,51]. For this investigation, the displacement of E_{corr} found for most of the acidic solution containing inhibitors against the blank solution of 1.0 M HCl is around ± 46 mV against the reference electrode (Ag|AgCl|Cl⁻) and shifted more to the anodic region Figure 7. Thus, it may be deduced *Uncaria Cordata* as a corrosion inhibitor, may be classified as a mixed corrosion inhibitor that preponderantly behaves as an anodic inhibitor.

Table 3 tabulates the η_{Rp} (%) based on the linear polarization resistance measurements in the ranges of 100 to 400 ppm in which inhibition efficiencies were found to increase from 89.0% to a maximum of 91.1%. Furthermore, LPR measurement also reveals the true corrosion rates in millimeters per year (mm/year) in which the corrosion rates may be ranked as follows: 100 ppm (4.02 mm/yr.) < 200 ppm (2.59 mm/yr.) < 300 ppm (2.23 mm/yr.) < 400 ppm (1.43 mm/yr.). Overall, based on both measurements tested at 400 ppm of inhibitors in the 1.0 M HCl, the dissolution rates of MS are potently enhanced as indicated by high inhibition corrosion efficiencies as opposed to blank solution.

3.3. Adsorption isotherm

The data gathered from polarization measurements are tested with different adsorption isotherms to establish high-prioritized formation on interactions between the adsorbed *Uncaria Cordata* active components with the metal/solution interface Figure 8. The surface coverage (θ) in the ranges of 100 to 400 ppm concentration for the inhibitors, as shown in Table 3 is derived from the equation [52,53]

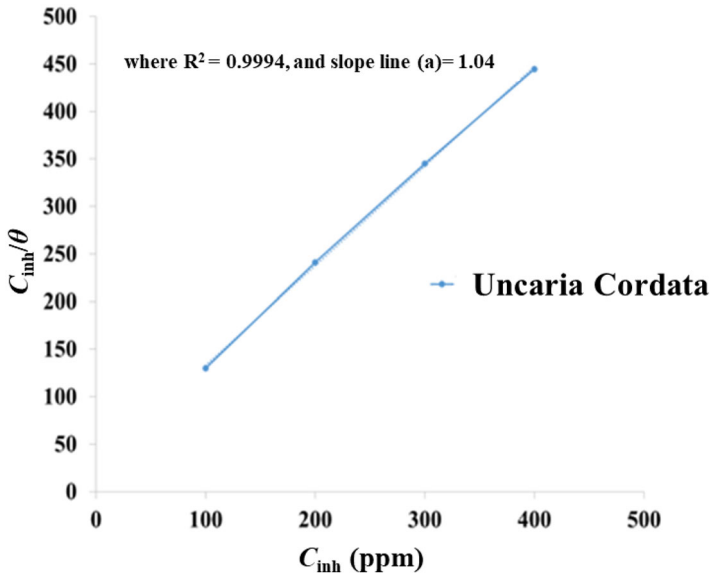


Figure 8. Langmuir adsorption isotherm for *Uncaria Cordata* on MS surface with and without the addition of inhibitor in 1.0 M HCl at 25 °C.

$$\theta = \frac{\eta_{pol}(\%)}{100} \quad (6)$$

where the $\eta_{pol}(\%)$ is the inhibition efficiency values for distinct concentrations of the tested inhibitors attained out of the polarization measurement. The best-fitted isotherm of the Langmuir adsorption isotherm is chosen, as demonstrated in Figure 8. The equation for Langmuir adsorption isotherm is expressed as in equation [52,53]

$$\frac{C_{inh}}{\theta} = \frac{1}{K_{ads}} + C_{inh} \quad (7)$$

in which θ is the constituents of the inhibitor's surface coverage (coverage proportion), C_{inh} concentration of the inhibitors, and K_{ads} is the equilibrium constant of the adsorption. The graph of C_{inh}/θ against C_{inh} produces linear lines, accompanied by a slope of almost near to the value of 1 (the value for the coefficient of regression found is 0.9994). The values for K_{ads} highly correlate to the standard free energy adsorption (ΔG_{ads}), by employing the calculation of [54,55]

$$\Delta G_{ads} = -RT \ln(55.5 K_{ads}) \quad (8)$$

where R delineates the gas constant, T is the absolute temperature, whereas 55.5 represents the water concentration (mol/L).

Typically, the deliberated values of ΔG_{ads} in the span of -20 kJ/mol until -40 kJ/mol indicate physisorption adsorption [39,56,57], with a negative sign for ΔG_{ads} deduces simultaneous adsorption as well as the steadiness for the adsorbed film on the top of the metal/solution interface [58,59]. The information collected from polarization measurements indicates that the considered value for ΔG_{ads} is

–19.70 kJ/mol, reviewing the adsorption scheme on the MS surface mostly due to the physisorption, and may as well mixed with chemical adsorption as suggested by [60]. In an aqueous phase, the “weak” standard adsorption-free energy is anticipated, as shown by the Monte Carlo simulation results. The ΔG_{ads} value is less exothermic (exergonic) due to the inhibitor molecules replacing water molecules from the MS surface and coordinating themselves on the surface [60]. Since the chemisorption is short ranged and directional, this will increase the contact area for the molecules on the MS surface to be chemisorbed by forming chemical bonds with the orbital of metal.

3.4. Atomic force microscopy (AFM)

The quantitative verification with respect to MS surface roughness without inhibitor and in the presence of *Uncaria Cordata* as corrosion inhibitors were inadequately investigated in SEM images. Thus, AFM measurement is highly competent in validating the impediment relating to the surface morphology of MS surface, especially in delivering information on surface roughness. Generally, the elevated values of surface roughness are indicated for significant dissolution of metal due to the attack of a corrosive solution to its metal surface by conveying an uneven surface expected from surface heterogeneity [61,62]. Figure 9 represents the 3D AFM images to explain the topography of MS under the influence of different exposure to the solution under examination. It was found the entropy of the surface for MS in the presence of 400 ppm of corrosion inhibitor is highly reduced in Figure 9(b) as compared to an uninhibited solution in Figure 9(a). The height profiles in Figure 10(a) show the serious deterioration of MS under corrosion which oxidized at a higher rate and resulted in greater surface roughness which is 113.410 nm. On the other hand, in Figure 10(b), after an optimum amount of *Uncaria Cordata* at 400 ppm in the tested corrosive medium, the surface roughness is notably decreased at 61.981 nm. In general, the inclusion of 400 ppm *Uncaria Cordata* inhibitor in the acidic solution reveals the surface of MS is better protected due to the formation of an enclosed film even

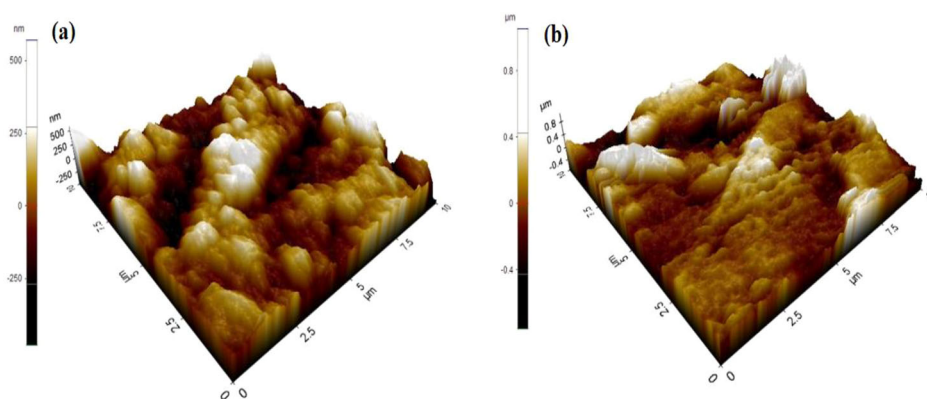


Figure 9. 3D AFM images of MS surface following the immersion for 24 h in (a) 1.0 M HCl and (b) 400 ppm of *Uncaria Cordata* in 1.0 M HCl.

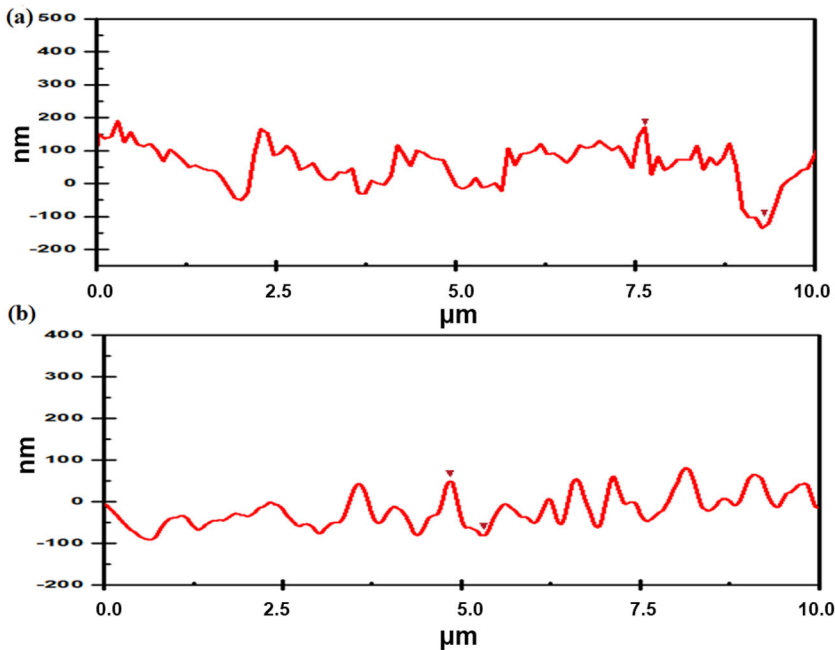


Figure 10. Height profiles of MS in 1.0 M HCl immersed in the span of 24 h for (a) uninhibited solution and (b) inhibited solution containing *Uncaria Cordata's* inhibitor at 400 ppm.

left to be exposed for the duration of 24 h, unlike the highly corroded MS solely immersed in the 1.0 M HCl.

3.5. Scanning electronic microscopy (SEM)/energy Dispersive X-Ray Spectroscopy (EDX)

As revealed in [Figure 11](#), the SEM illustration depicted the MS metal/aqueous acidic solution interface in the former and later of 24 h immersion in 1.0 M HCl solution. [Figure 11\(a\)](#) illustrates the serious disintegration of the MS surface, as well as exhibits an irregularity on account of zero protection from inhibitors. The microstructural studies for MS after immersion in 1.0 M HCl solution containing 400 ppm corrosion inhibitor reveal the MS surface endures uniform corrosion mostly due to the high concentration of hydronium (H_3O^+) ions in the solution and affect severely for the MS surface in the absence of an inhibitor. Thus, the inclusion of 400 ppm of *Uncaria Cordata* in the 1.0 M HCl greatly improved the MS surface in terms of its uniformity and appearance ([Figure 11\(b\)](#)). The adsorption of the inhibitor's active components at the MS metal/surface by forming an almost unperturbed insulating film from the destructive invasion of acidic compounds in the electrolyte effectively protects the underneath MS from corroding at a much higher rate [63,64].

[Figure 12](#) illustrates the SEM/EDX, which is used to confirm the creation of the protective film owing to inhibitor adsorption on the surface of MS [65]. [Figure 12](#) illustrates a much higher growth of iron oxides on the metal surface, indicates by the extremely high percentage composition of oxygen, O, in an uninhibited 1.0 M HCl

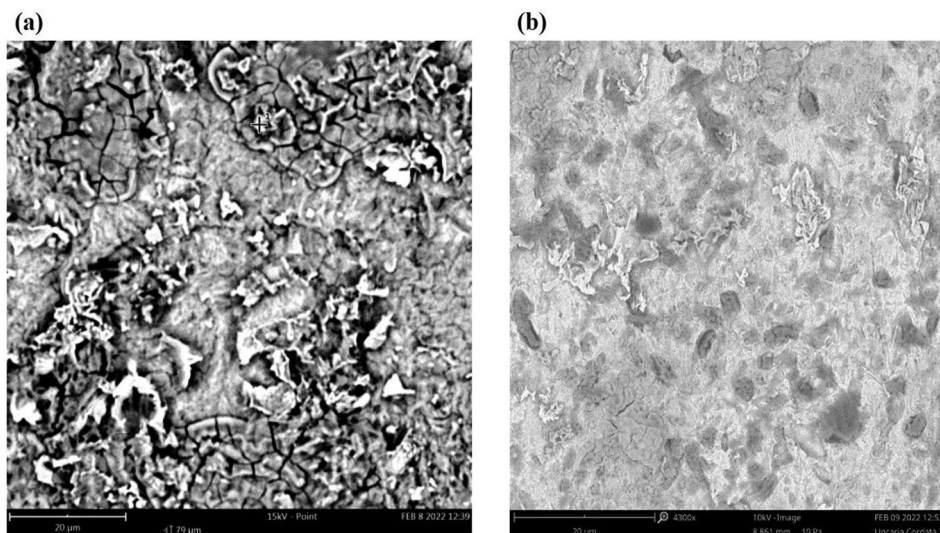


Figure 11. SEM micrographs for MS surface in (a) blank solution and (b) filled with *Uncaria Cordata* at 400 ppm after 24 h of immersion in 1.0 M HCl.

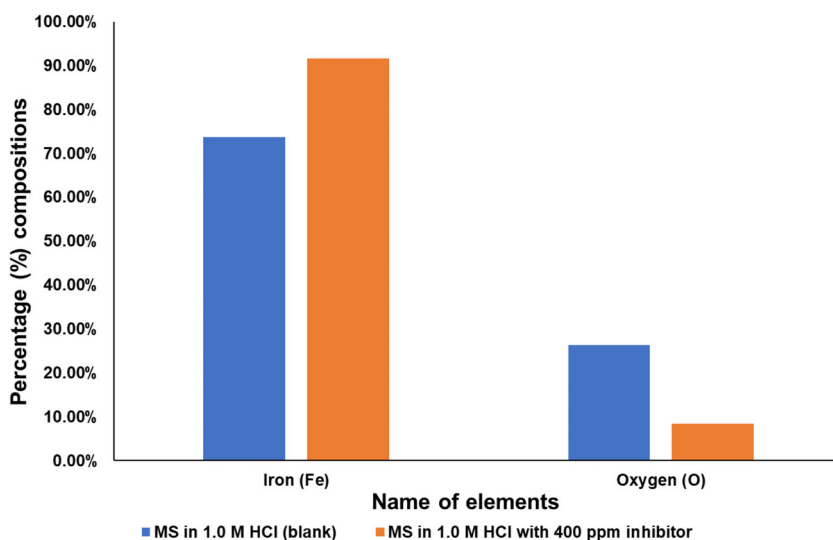


Figure 12. Percentage (%) compositions of elements as corrosion products present on MS surface after 24 h of immersion in 1.0 M HCl solution and 400 ppm inhibitor in 1.0 M HCl solution.

solution (26.32%) as opposed to MS immersed in 400 ppm of *Uncaria Cordata* extract (8.45%) in 1.0 M HCl solution [66,67]. The Fe percentage composition is decreasing in relation to the uninhibited MS surface sample (73.68%) and is high in 400 ppm of corrosion inhibitors (91.55%). Next, Figure 13 shows the elemental distribution of corrosion products in respect of Fe and O are enhanced or reduced in varying sections after 24 h of MS immersion in the corrosive solution with or without the addition of a 400 ppm inhibitor. Remarkably, the increase in the Fe elemental distribution is proof that an insulation layer has formed on the MS surface containing

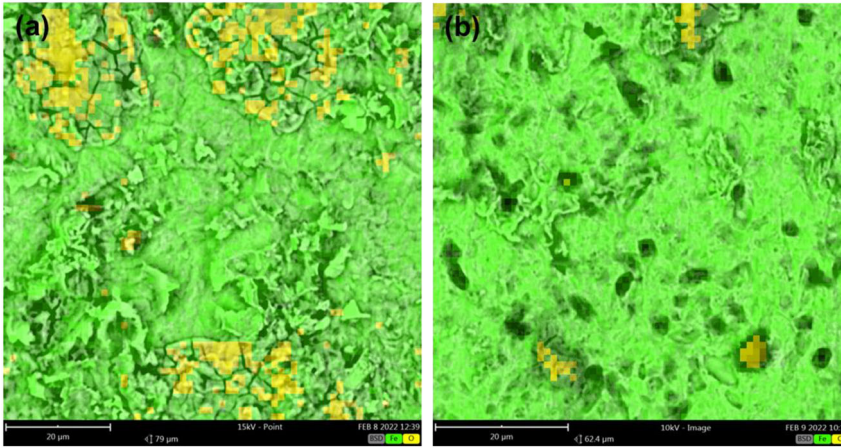


Figure 13. The elemental distribution maps of Fe (■) and O (■) on the MS surface after immersion in (a) 1.0 M HCl and (b) 1.0 M HCl with 400 ppm of inhibitor.

400 ppm of the inhibitor even though the MS was completely immersed for 24 h in the corrosive solution as opposed to the blank solution [68,69]. The SEM/EDX analyses confirm findings from polarization and linear polarization resistance measurements, which highly suggest that a protective film was formed over the MS surface, hence retarded both anodic and cathodic reactions.

3.6. Density functional theory (DFT)

The reactivity of the molecular arrangement is established on the frontier molecular orbitals theory, where the frontier molecular orbital energies were determined comparatively to Koopmans' Theorem [70,71], where E_{HOMO} and E_{LUMO} of the active components are linked to the ionization potential, $I = -E_{\text{HOMO}}$ and electron affinity, $A = -E_{\text{LUMO}}$. Other quantum chemical restrictions such as electronegativity (χ), hardness (η), and softness (σ) were approximated as per the following equations [72–74]:

$$\chi = \frac{I + A}{2} \quad (9)$$

$$\eta = \frac{1}{2} \left(\frac{\partial \mu}{\partial N} \right)_v = \frac{1}{2} \left(\frac{\partial^2 \mu}{\partial N^2} \right)_v = \frac{(I - A)}{2} \quad (10)$$

$$\sigma = \frac{1}{\eta} \quad (11)$$

The electrons portion shifted toward the metallic surface from the inhibitor, ΔN was determined using Equation (12) as follows [75]:

$$\Delta N = \frac{\varphi_{\text{Fe}} - \chi_{\text{inh}}}{2(\eta_{\text{Fe}} + \eta_{\text{inh}})} \quad (12)$$

Table 4. Computed quantum chemical parameters of selected active components in their ground state calculated at B3LYP/DNP.

Compound	Abbreviation	E_{HOMO} (eV)	E_{LUMO} (eV)	ΔE (eV)	χ (eV)	σ (eV) ⁻¹	ΔN
Quercetin	1	-5.566	-1.832	3.734	1.867	3.699	0.298
Kaempferol	2	-5.624	-1.783	3.841	1.921	3.704	0.288
Scopoletin	3	-5.990	-1.883	4.107	2.054	3.937	0.213
Taxifolin	4	-5.892	-1.700	4.192	2.096	3.796	0.242
3,4-dihydroxybenzoic acid	5	-6.334	-1.411	4.923	2.462	3.873	0.245
2-hydroxybenzoic acid	6	-6.613	-1.493	5.120	2.560	4.053	0.190
2,4-dihydroxybenzoic acid	7	-6.565	-1.246	5.319	2.660	3.906	0.148
Loganin	8	-6.452	-0.853	5.599	2.800	3.653	0.170
β -sitosterol	9	-6.251	0.707	6.958	3.479	2.772	0.207

where $\Phi_{\text{Fe}(110)}$ is the work function of Fe(110) surfaces, χ_{inh} denotes the pure electronegativity of the inhibitor molecule; and η_{Fe} and η_{inh} are the pure hardness of iron and the inhibitor molecule, correspondingly.

The deliberated quantum chemical parameters of the active components identified in *Uncaria Cordata* in their ground state are given in Table 4. HOMO (highest occupied molecular orbital) – LUMO (lowest unoccupied molecular orbital) are investigated to assess the nature of donor-acceptor interaction, where the estimation of E_{HOMO} indicates the ability to contribute electrons and E_{LUMO} specifies the tendency to acquire electrons [76,77]. The calculated results in Table 4 are sorted from lowest to highest energy gap, $\Delta E = E_{\text{LUMO}} - E_{\text{HOMO}}$, which is unequaled crucial energy parameters in assessing corrosion inhibitor reactivity towards a metal surface during adsorption. A lesser value of ΔE will improve the inhibitory effect as the mutual interaction between the iron surface and the active components improved [78,79].

In theory, the high inhibition effectiveness of *Uncaria Cordata* extract is on the account of the existence of compounds with high E_{HOMO} and low E_{LUMO} values. For example, we take **8**, which was originally discovered in the genus *Uncaria Cordata* genus, as well as **2** and **1** [15], which have favorable electronic properties as our compounds of interest. Based on the results obtained from the DFT calculations, the respective E_{HOMO} values for compounds **8**, **2**, and **1** are as follows: **8** (–6.452 eV), **2** (–5.624 eV), and **1** (–5.566 eV), whereas calculated E_{LUMO} values are demonstrated as: **8** (–0.853 eV), **2** (–1.783 eV), and **1** (–1.832 eV). The increase and decrease in E_{HOMO} and E_{LUMO} values correspond to the molecules' enhanced potential to emit and gain electrons when interacting with a metal surface [80].

Figure 14 illustrates the optimized geometry of **1**, **2**, and **8** and their respective distribution of HOMO and LUMO orbitals. The figure explicitly shows that the molecular orbitals HOMO and LUMO for **1** and **2** are distributed all over the molecule structures. The HOMO orbitals in **1** and **2** are localized mainly at the benzene function, hydroxy (–OH), and carbonyl groups (C–O, C=O). The availability of heteroatom oxygen and several functional groups suggest possible transfer of electrons from the unbonded electrons and π -electrons to the unfilled $3d$ orbitals of the iron cations, hence enhancing the inhibition proficiency. Additionally, the LUMO orbital is localized over all molecular structures of **1** and **2**, which assist the adsorption of the extracts' active components on the iron surface by accepting electrons from the

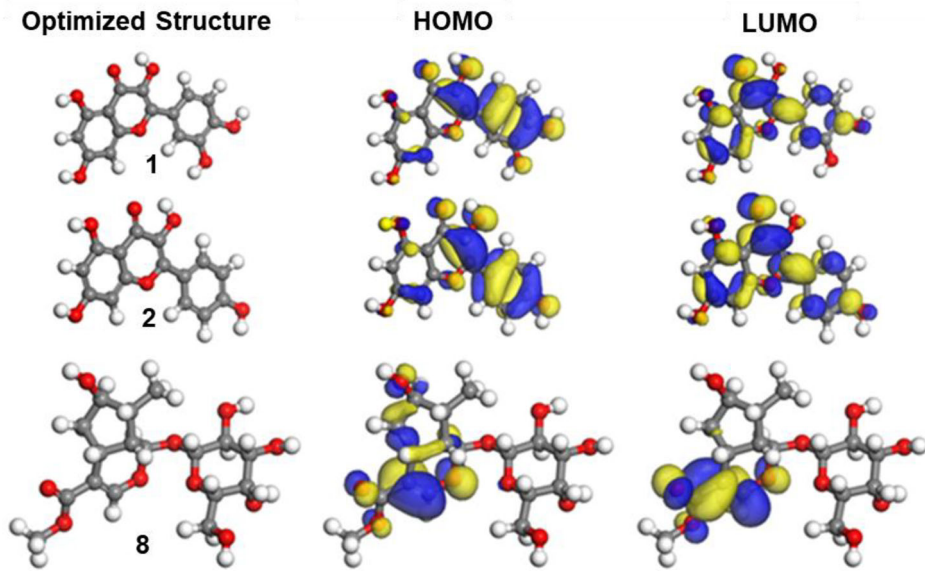


Figure 14. Optimized geometry and isosurface densities of HOMOs and LUMOs of molecules **1**, **2**, and **8**.

occupied iron orbitals [81]. For **8**, the HOMO and LUMO orbitals are scattered primarily on the functional molecular group with an indene chemical structure.

3.7. Monte Carlo simulation

The adsorption characteristics of **1**, **2**, and **8** were analyzed by conducting a Monte Carlo simulation to study their adsorption characteristics. Figure 15 depicts that all three active compounds in the extract are adsorbed side by side toward the iron surface in a vacuum, maximizing the surface coverage. This propounds the establishment of a shielded layer by the active components to protect the metal surface from corrosive agents. The negative adsorption energy of **1** (−156.183 kcal/mol), **2** (−151.690 kcal/mol), and **8** (−183.004 kcal/mol) propose that adsorption of the active components occurs naturally on the iron surface. The finding follows the outcomes from DFT calculations, suggesting **1** is more reactive than **2**. On the contrary, **8** has the lowest adsorption energy, probably due to the molecule's size, which allows it to form multiple weak physisorption interactions with the metal surface, especially in a solid/gas interface [82,83].

We conduct a further simulation to explore the adsorption behavior of the three active components on an iron surface in the availability of water as well as credible corrosive agents. Thus, 600 water molecules, 6 hydronium ions H_3O^+ , and 6 chloride ions Cl^- were added into the simulation bounding box to simulate the corrosive environment of 1.0 M HCl. As explained earlier, the negative values for the total and individual adsorption energy of the three active components in their stable form suggest instinctive adsorption of the molecules over the iron surface, even in corrosive media. As tabulated in Table 5, we can deduce that the inhibition performance of **1**

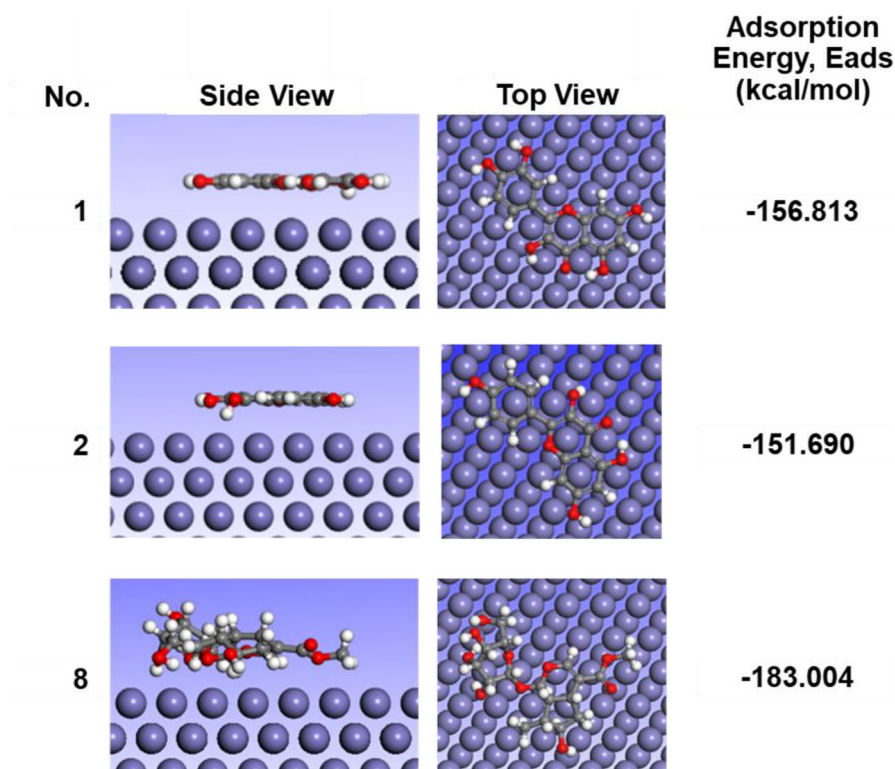


Figure 15. Equilibrium orientation of the utmost stable conformation of **1**, **2**, and **8** in their neutral structure on Fe (110).

Table 5. Energy parameters in kcal/mol for the most stable adsorption configurations for **1**, **2**, and **8** in their neutral conformation on Fe (110) surface in 1.0M HCl.

Molecules	1	2	8
Total energy	-8,829.183	-8,896.223	-8,740.621
Adsorption energy	-8,888.986	-8,947.876	-8,861.038
Rigid adsorption energy	-9,167.026	-9,240.688	-9,156.461
Deformation energy	278.039	292.812	295.423
Inh: dE _{ads} /dNi	-221.131	-215.040	-124.310
H ₂ O: dE _{ads} /dNi	-0.473	-0.736	-0.540
Cl ⁻ : dE _{ads} /dNi	-147.885	-146.433	-151.210
H ₃ O ⁺ : dE _{ads} /dNi	-173.377	-141.881	-164.750

and **2** against the iron surface immersed in an acidic medium is enhanced. The individual adsorption energy for **1** and **2** decreased to -221.131 kcal/mol and -215.040 kcal/mol from -156.183 kcal/mol and -151.690 kcal/mol, respectively, whilst the individual adsorption energy for **8** increased from -183.004 kcal/mol, to -124.310 kcal/mol. These results correlate with DFT calculations suggesting **1** is more reactive than **2**, and **8** has lesser reactivity towards a metal surface.

Figure 16 compares the individual adsorption energy of the corrosion inhibitor's active compounds plus the ions of Cl⁻ and H₃O⁺. We can relate that apart from **8**, **1** and **2** show remarkable adsorption performance compared to Cl⁻ and H₃O⁺. The finding suggests that **1** and **2** found in *Uncaria Cordata* extract can form a protective

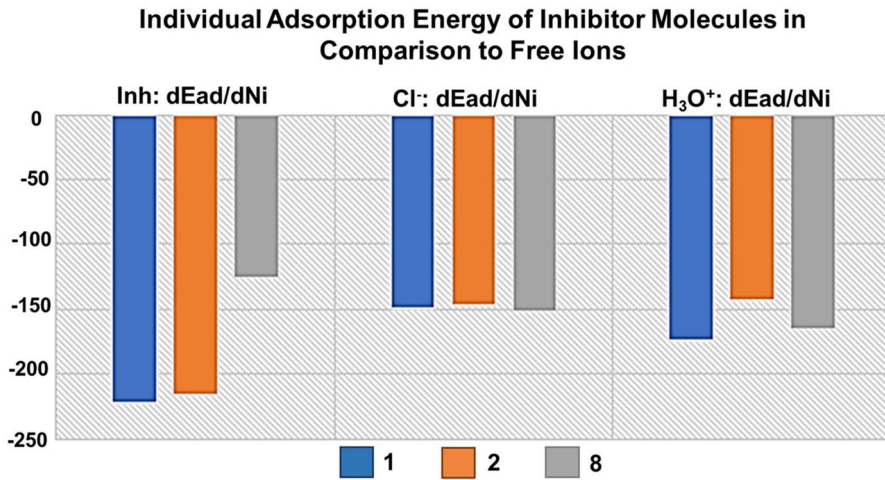


Figure 16. The individual adsorption energy of 1, 2, and 8 in comparison to free ions in 1.0M HCl solution.

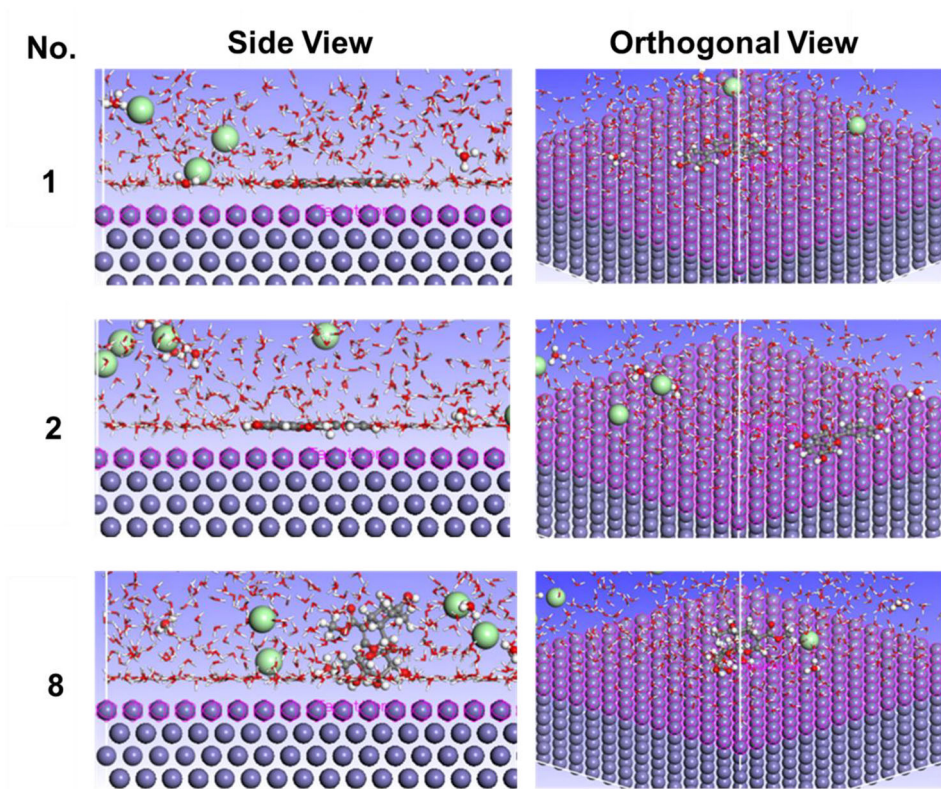


Figure 17. Adsorption configurations of 1, 2, and 8 in 1.0M HCl solution.

layer against corrosive agents by gradually replacing water molecules, Cl⁻ and H₃O⁺ ions in an aqueous acidic solution. The small-energy adsorption conformations of the corrosion inhibitor’s molecules in 1.0M HCl solution are presented in [Figure 17](#). It

can be noted that **1** and **2** molecules adsorbed on the metal top surface in a flat layout, which improves the surface coverage and signifies the corrosion inhibition achievement, which was reinforced by the earliest findings for **1** to achieve as high as 98% as corrosion inhibitor for C38 in HCl solution [84], whereas up to 96% for **2** to inhibit corrosion on MS in the HCl medium [85].

3.8. Adsorption mechanism

Heterocyclic compounds in the *Uncaria Cordata* plant greatly contribute to the adsorption sites on MS by slowing down the corrosion rates of metal in 1.0 M HCl solution [3]. As the inhibition efficiencies depend on the high individual adsorption energy of the corrosion inhibitor's active compounds of **1**, **2**, and **8**, we have proposed a plausible adsorption mechanism involving the respective active compounds in Figure 18. The retardation of the corrosion reaction is due to the interaction of π electrons in the cyclic ring as well as the O atom as the electron donor group in all of the active component's molecule structures with the orbital of Fe. Each active component's molecule in the *Uncaria Cordata* may form a protective film on the MS surface *via* a lone O atom and in the polar conjugated bond of C to the O (C=O). These factors aid most of the active compound's molecules, as found in Figure 1, particularly the active compounds of **1**, **2**, and **8** to donate electrons from the heterocyclic compound to the empty $3d$ orbital of the metal substrate, thus forming coordinate covalent bonds. The inductive effect may form *via* the σ electrons due to the substituents' electronegativity, in which the electrons shift toward the carbonyl group (C=O). The effect is more pronounced in the electron-donating groups, such as the methyl ($-\text{CH}_3$) group. On the other hand, for an electron-donating group, for example, the hydroxyl ($-\text{OH}$) group will activate the benzene ring through the resonance effect. Since the active components in the corrosion inhibitor contain a high number of

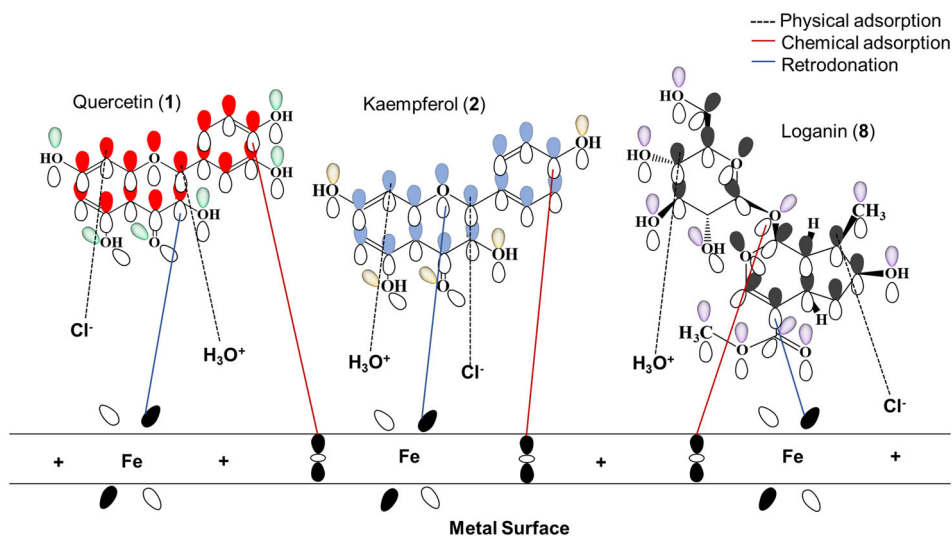


Figure 18. The proposed adsorption mechanism of the **1**, **2**, and **8** compounds at the metal/solution interface in 1.0 M HCl.

-OH groups which attributes to the delocalization of π -electrons, the molecules are stable in the acidic solution and provide greater protection in shielding the metal surface from corrosion [86]. Generally, the dissociation of HCl (strong acid) in the aqueous solution produces chloride (Cl^-) ions and hydronium (H_3O^+) in which most of the ions will be in the aqueous solution, and a lower amount is attracted to the positively charged MS surface. The results in SEM highly indicate that the Cl^- ions have the lesser effect on impeding the corrosion of the MS surface, as H_3O^+ ions are the main components in accelerating the corrosion reaction. In DFT, molecule **1** is more reactive than **2**, thus it may form physical adsorption, whereas **8** has the lowest adsorption energy (bigger molecule's size), which allows it to have more adsorption centers but a weaker form of physical adsorption interactions with the metal surface. As discussed earlier in the Monte Carlo simulation, molecules **1** and **2** have a higher tendency to form an insulating film against corrosive agents by progressively replacing water molecules, Cl^- and H_3O^+ ions on the MS surface. Furthermore, chemical adsorption, which is naturally formed between the inhibitor's molecules to the MS surface, is due to the electron donation from the filled orbital electrons in the organic molecules with the vacant $3d$ orbital of the Fe atoms. In return, the filled orbital Fe atoms will donate back the electrons to the orbital of the inhibitor molecule by back bonding (retrodonation) [87,88].

4. Conclusion

The *Uncaria Cordata* as a corrosion inhibitor on MS is effective in reducing the corrosion rate of MS in 1.0 M HCl medium at 25 °C.

1. The findings in polarization measurement indicate the corrosion inhibitor's active compounds are adsorbed on the surface of MS in the corrosive medium. The increase of concentration of the inhibitors minimizes current densities of anodic and cathodic reactions, in addition, shifts the corrosion potential towards the noble position and recommends slowing down of MS dissolution reaction.
2. The corrosion inhibition efficiencies for the *Uncaria Cordata* measured in the EIS, polarization, and linear polarization measurements reach agreement at 400 ppm is the ideal concentration for the corrosion inhibitors to reach maximum inhibition and reached a plateau beyond the concentration.
3. The adsorption adheres to Langmuir adsorption isotherm and ΔG_{ads} is specified above.
4. The SEM/EDX and AFM revealed film determined by the *Uncaria Cordata* on the MS surface greatly improves the condition of the MS surface appearances as opposed to the bare MS fully immersed in 1.0 M HCl.
5. The correlation of the corrosion inhibition efficiency with the electronic properties of nine active compounds that are present in the *Uncaria Cordata* inhibitor was established by DFT calculations. The lower calculated ΔE values promote improvement in the inhibition performance, thus suggesting a synergy mechanism for most of the adsorbed active compounds in *Uncaria Cordata* inhibitors with the MS surface.

6. The adsorption features of selected active compounds from *Uncaria Cordata*, namely **1**, **2**, and **8**, were further investigated by Monte Carlo simulation. *Uncaria Cordata* have parallel adsorption on MS which boosts maximum surface coverage. Furthermore, it verifies theoretically the establishment of a protecting film by the *Uncaria Cordata* active components to shield the MS surface from the intrusion of free ions in the 1.0 M HCl solution. The finding is tallied with the results from DFT calculations signifying **1** is more reactive than **2**, while **8** has the least adsorption energy.
7. The adsorption mechanism for the **1**, **2**, and **8** in *Uncaria Cordata* extract involves physical and chemical adsorption.

Acknowledgement

This work was supported by the Universiti Teknologi MARA (UiTM) under Grant 100-RMC 5/3/SRP (094/2021) and 600-RMC/MyRA 5/3/LESTARI (011/2020).

Author contributions

Nor Affanizam Othman: Visualization, Formal analysis, Methodology, Software, Data Curation, Writing - Original Draft. Ab Malik Marwan Ali: Resources. Noor Syafiqah Samsi: Methodology, Investigation, Data Curation. Fatimah Salim: Resources. Dedikarni Panuh: Funding acquisition. Muhamad Kamil Yaakob: Supervision, Software, Validation. Zaidi Embong: Supervision, Writing- Reviewing and Editing, Ahmad Shalabi Md Sauri: Resources. Nik Norziehana Che Isa: Funding acquisition. Nor Zakiah Nor Hashim: Supervision, Conceptualization, Validation, Visualization, Project administration.

Disclosure statement

No potential conflict of interest was reported by the author(s).

Data availability

The raw/processed data required to reproduce these findings cannot be shared at this time as the data also forms part of an ongoing study.

References

- [1] Sheetal; Batra R, Singh AK, Singh M, et al. Advancement of corrosion inhibitor system through N-Heterocyclic compounds: a review. *Corros Eng Sci Technol.* 2022; 58(1):73–101.
- [2] Gerengi H, Cabrini M, Solomon MM, et al. Assessment of the corrosion behaviour of untreated and chemically treated pure magnesium in simulated body fluid. *J Adhes Sci Technol.* 2022;1–17.
- [3] Wang X, Chen L, Yang F, et al. Corrosion inhibition mechanism and extraction technology of plant corrosion inhibitors: a review. *J Adhes Sci Technol.* 2023;:1–25.
- [4] Al-Moubaraki AH, Al-Malwi SD. Experimental and theoretical evaluation of aqueous black mustard seeds extract as sustainable-green inhibitor for mild steel corrosion in H₂SO₄ acid solutions. *J Adhes Sci Technol.* 2022;36(23–24):2612–2643.

- [5] Zhang Q, Zhang R, Wu R, et al. Green and high-efficiency corrosion inhibitors for metals: a review. *J Adhes Sci Technol*. 2022;1–24.
- [6] Cheng CR, Emori W, Wei K, et al. Natural triterpenoids of *Ganoderma lucidum* as new, green, and effective corrosion inhibitor for steel in acidic medium: characterization, experimental and theoretical investigations. *J Adhes Sci Technol*. 2022;36(23–24): 2708–2731.
- [7] Namitha K, Rao P, Rao SA. A brief insight into the use of plant products as green inhibitors for corrosion mitigation of aluminium and aluminium alloys. *Can Metall Q*. 2022;61(4):429–441.
- [8] Raju LK, Mana GK, Cheruthazhakkatt S, et al. Phytochemical contents and *in vitro* antioxidant activities of aqueous, hydroalcoholic and methanolic extracts of shankhpushpi (*Clitoria ternatea*. L) Plant cultivated under polyhouse and open field conditions. *J Herbs Spices Med Plants*. 2022;28(3):217–236.
- [9] Usman I, Hussain M, Imran A, et al. S. Traditional and innovative approaches for the extraction of bioactive compounds. *Int J Food Prop*. 2022;25(1):1215–1233.
- [10] Jessima SJHM, Berisha A, Srikandan SS, et al. Preparation, characterization, and evaluation of corrosion inhibition efficiency of sodium lauryl sulfate modified chitosan for mild steel in the acid pickling process. *J Mol Liq*. 2020;320:114382.
- [11] Daoudi W, Guo L, Azzouzi M, et al. Evaluation of the corrosion inhibition of mild steel by newly synthesized imidazo[1,2-a]pyridine derivatives: experimental and theoretical investigation. *J Adhes Sci Technol*. 2023;1–24.
- [12] Bahadori A. *Essentials of Coating, Painting, and Lining for the Oil, Gas and Petrochemical Industries*. Amsterdam: Elsevier; 2015.
- [13] Solomon MM, Uzoma IE, Olugbuyiro JAO, et al. A censorious appraisal of the oil well acidizing corrosion inhibitors. *J Pet Sci Eng*. 2022;215:110711.
- [14] Kam TS. Alkaloids from Malaysian flora. *Alkaloids: chemical and biological perspectives*. 1999;14(C):285–435.
- [15] Abdullah NH, Salim F, Ahmad R. Cordata Var Ferruginea and their *in vitro* α -glucosidase inhibitory activities. *Molecules*. 2016;21(5):525. .
- [16] Hussin MH, Kassim MJ. The corrosion inhibition and adsorption behavior of uncaria gambir extract on mild steel in 1 M HCl. *Mater Chem Phys*. 2011;125(3):461–468.
- [17] Shojaee S, Shahidi Zandi M, Rastakhiz N. The effect of tetracycline drug as a green corrosion inhibitor for carbon steel in HCl media. *J Indian Chem Soc*. 2022;99(10):100700.
- [18] Sherif ESM. A comparative study on the electrochemical corrosion behavior of iron and X-65 steel in 4.0 Wt % sodium chloride solution after different exposure intervals. *Molecules*. 2014;19(7):9962–9974.
- [19] Roscher J, Liu D, Holze R. A comparison of methods for corrosion inhibitor assessment: mild steel protected by disubstituted aromatics. *Mat Corr*. 2022;73(2):254–258.
- [20] Finšgar M, Jackson J. Application of corrosion inhibitors for steels in acidic media for the oil and gas industry: a review. *Corros Sci*. 2014;86:17–41.
- [21] Kosareva EK, Pivkina AN, Muravyev N. V Atomic force microscopy in energetic materials research: a review. *Energetic Materials Frontiers*. 2022;3(4):290–302.
- [22] Baskar P, Rathinapriya P, Prabakaran M. Use of trochodendron aralioides extract as green corrosion inhibitor for mild steel in 1M HCl solutions. *Processes* 2022, Vol. 10, Page 1480. 2022;10(8):1480.
- [23] Hashim NZN, Anouar EH, Kassim K, et al. XPS and DFT investigations of corrosion inhibition of substituted benzylidene schiff bases on mild steel in hydrochloric acid. *Appl Surf Sci*. 2019;476:861–877.
- [24] Zaidon FH, Kassim K, Mohd Zaki H, et al. Adsorption and corrosion inhibition accomplishment for thiosemicarbazone derivatives for mild steel in 1.0 M HCl medium: electrochemical, XPS and DFT studies. *J Mol Liq*. 2021;329:115553.
- [25] Hashim NZN, Kahar MAM, Kassim K, et al. Experimental and theoretical studies of azomethines derived from benzylamine as corrosion inhibitors of mild steel in 1 M HCl. *J Mol Struct*. 2020;1222:128899.

- [26] Olasunkanmi LO, Idris AO, Adewole AH, et al. Adsorption and corrosion inhibition potentials of salicylaldehyde-based schiff bases of semicarbazide and p-Toluidine on mild steel in acidic medium: experimental and computational studies. *Surf Interfaces*. 2020;21:100782.
- [27] Kasprzhitskii A, Lazorenko G. Corrosion inhibition properties of small peptides: DFT and monte carlo simulation studies. *J Mol Liq*. 2021;331:115782.
- [28] Elbelghiti M, Karzazi Y, Dafali A, et al. Experimental, quantum chemical and monte carlo simulation studies of 3,5-disubstituted-4-amino-1,2,4-triazoles as corrosion inhibitors on mild steel in acidic medium. *J Mol Liq*. 2016;218:281–293.
- [29] Alhaffar MT, Umoren SA, Obot IB, et al. Studies of the anticorrosion property of a newly synthesized green isoxazolidine for API 5L X60 steel in acid environment. *J Mater Res Technol*. 2019;8(5):4399–4416.
- [30] Ferigita KSM, AlFalah MGK, Saracoglu M, et al. Corrosion behaviour of new Oxo-Pyrimidine derivatives on mild steel in acidic media: experimental, surface characterization, theoretical, and monte carlo studies. *Applied Surface Science Advances*. 2022;7:100200.
- [31] John S, Joseph A, Sajini T, et al. Corrosion inhibition properties of 1,2,4-hetrocyclic systems: electrochemical, theoretical and Monte Carlo simulation studies. *Egypt J Pet*. 2017;26(3):721–732.
- [32] Moradi M, Ghiara G, Spotorno R, et al. Understanding biofilm impact on electrochemical impedance spectroscopy analyses in microbial corrosion and microbial corrosion inhibition phenomena. *Electrochim Acta*. 2022;426:140803.
- [33] Vashishth P, Bairagi H, Narang R, et al. Thermodynamic and electrochemical investigation of inhibition efficiency of green corrosion inhibitor and its comparison with synthetic dyes on MS in acidic medium. *J Mol Liq*. 2022;365:120042.
- [34] Mehta RK, Gupta SK, Yadav M. Studies on pyrimidine derivative as green corrosion inhibitor in acidic environment: electrochemical and computational approach. *J Environ Chem Eng*. 2022;10(5):108499.
- [35] Bhardwaj N, Sharma P, Singh K, et al. Phyllanthus emblica seed extract as corrosion inhibitor for stainless steel used in petroleum industry (SS-410) in acidic medium. *Chemical Physics Impact*. 2021;3:100038.
- [36] Lima KCDSd, Paiva VM, Perrone D, et al. Glycine max meal extracts as corrosion inhibitor for mild steel in sulphuric acid solution. *J Mater Res Technol*. 2020;9(6):12756–12772.
- [37] Farag ZR, Moustapha ME, Anouar EH, et al. The inhibition tendencies of novel hydrazide derivatives on the corrosion behavior of mild steel in hydrochloric acid solution. *J Mater Res Technol*. 2022;16:1422–1434.
- [38] Jeeja Rani AT, Sreelakshmi T, Joseph A. Effect of the addition of potassium iodide and thiourea on the corrosion inhibition effect of aqueous extract of *Ayapana triplinervis* towards mild steel in HCl at elevated temperatures-theoretical, electrochemical and surface studies. *J Mol Liq*. 2022;366:120211.
- [39] Ganjoo R, Sharma S, Thakur A, et al. Experimental and theoretical study of sodium cocoyl glycinate as corrosion inhibitor for mild steel in hydrochloric acid medium. *J Mol Liq*. 2022;364:119988.
- [40] Ellis G. Review of the frequency domain. *Observers in Control Systems*. 2002; p 41–66.
- [41] Zuñiga-Díaz J, Reyes-Dorantes E, Quinto-Hernandez A, et al. Biodiesel from “Morelos” rice: synthesis, oxidative stability, and corrosivity. *J Chem*. 2018;2018:1–11.
- [42] Habeeb HJ, Luaibi HM, Abdullah TA, et al. A case study on thermal impact of novel corrosion inhibitor on mild steel. *Case Stud Therm Eng*. 2018;12:64–68.
- [43] Sanni O, Popoola AP. I. Data on environmental sustainable corrosion inhibitor for stainless steel in aggressive environment. *Data Brief*. 2019;22:451–457.
- [44] Hamani H, Daoud D, Benabid S, et al. Electrochemical, density functional theory (DFT) and molecular dynamic (MD) simulations studies of synthesized three news

- schiff bases as corrosion inhibitors on mild steel in the acidic environment. *J Indian Chem Soc.* 2022;99(7):100492.
- [45] Ituen E, Akaranta O, James A. Corrosion inhibition characteristics of 2-[(E)-[5-Methoxy-1-[4-(trifluoromethyl)phenyl]pentylidene]amino]oxyethanamine on steel in simulated oilfield acidizing solution. *J King Saud Univ.* 2019;31(2):191–199.
- [46] Laamari MR, Benzakour J, Berrekhis F, et al. Adsorption and corrosion inhibition of carbon steel in hydrochloric acid medium by hexamethylenediamine tetra(methylene phosphonic acid). *Arabian J Chem.* 2016;9: S245–S251.
- [47] Cotting F, Aoki IV. Octylsilanol and Ce(III) ions – alternative corrosion inhibitors for carbon steel in chloride neutral solutions. *J Mater Res Technol.* 2020;9(4):8723–8734.
- [48] Kusumaningrum I, Soenoko R, Siswanto E, et al. Investigation of *Artocarpus heterophyllus* peel extract as non-toxic corrosion inhibitor for pure copper protection in nitric acid. *CSCEE.* 2022;6:100223.
- [49] Al-Amiery AA, Ahmed MHO, Abdullah TA, et al. Electrochemical studies of novel corrosion inhibitor for mild steel in 1 M hydrochloric acid. *Results Phys.* 2018;9:978–981.
- [50] Sanni O, Ren J, Jen T-C. Agro-Industrial wastes as corrosion inhibitor for 2024-T3 aluminum alloy in hydrochloric acid medium. *Results Eng.* 2022;16:100676.
- [51] Sanni O, Ren J, Jen TC. Understanding the divergence of agro waste extracts on the microstructure, mechanical, and corrosion performance of steel alloy. *S Afr J Chem Eng.* 2022;40:57–69.
- [52] Rao S, R S, M M, et al. Experimental and DFT explorations of tert-butyl(1-(2-(4-nitrobenzylidene)-hydrazinyl)-1-oxopropan-2yl)-carbamate on CRCA metal in 1M HCl solution. *Res Surf Interfaces.* 2022;6:100024.
- [53] Ofuyekpone OD, Utu OG, Onyekpe BO. Corrosion inhibition for alloy 304L (UNS S30403) in H₂SO₄ 1M solution by *Centrosema pubescens* leaves extract. *APSADV.* 2021;3:100061.
- [54] El-Katori EE, El-Saeed RA, Abdou MM. Anti-corrosion and anti-microbial evaluation of novel water-soluble bis azo pyrazole derivative for carbon steel pipelines in petroleum industries by experimental and theoretical studies. *Arabian J Chem.* 2022;15(12): 104373.
- [55] Ishak A, Adams FV, Madu JO, et al. Corrosion inhibition of mild steel in 1M hydrochloric acid using haematostaphis barteri leaves extract. *Procedia Manuf.* 2019;35: 1279–1285.
- [56] Roth E, Mancier V, Fabre B. Adsorption of cadmium on different granulometric soil fractions: influence of organic matter and temperature. *Geoderma.* 2012;189–190: 133–143.
- [57] Ogunleye OO, Arinkoola AO, Eletta OA, et al. Green corrosion inhibition and adsorption characteristics of *Luffa cylindrica* leaf extract on mild steel in hydrochloric acid environment. *Heliyon.* 2020;6(1):e03205. [e03205](#).
- [58] Karthikaiselvi R, Subhashini S. Study of adsorption properties and inhibition of mild steel corrosion in hydrochloric acid media by water soluble composite poly (vinyl alcohol-o-methoxy aniline). *J Assoc Arab Univ Basic Appl Sci.* 2014;16(1):74–82.
- [59] Hameed RSA, Obeidat S, Qureshi MT, et al. Silver nanoparticles – expired medicinal drugs waste accumulated at hail city for the local manufacturing of green corrosion inhibitor system for steel in acidic environment. *J Mater Res Technol.* 2022; 21:2743–2756.
- [60] Kokalj A. Corrosion inhibitors: physisorbed or chemisorbed? *Corros Sci.* 2022;196: 109939.
- [61] Zhang X M, Chen Z y, Luo H F, et al. Corrosion resistances of metallic materials in environments containing chloride ions: a review. *Trans Nonferrous Met Soc China* 2022;32(2):377–410.
- [62] Bedmar J, Abu-Warda N, García-Rodríguez S, et al. Influence of the surface state on the corrosion behavior of the 316 L stainless steel manufactured by laser powder bed fusion. *Corros Sci.* 2022;207:110550.

- [63] de Damborenea J, Conde A, Arenas MA. Corrosion inhibition with rare earth metal compounds in aqueous solutions. *Rare Earth-Based Corrosion Inhibitors*. 2014;84–116.
- [64] Calle LM, Li W. Microencapsulated indicators and inhibitors for corrosion detection and control. *Handbook of Smart Coatings for Materials Protection*. 2014;:370–422.
- [65] Bellal Y, Benghanem F, Keraghel S. A new corrosion inhibitor for steel rebar in concrete: synthesis, electrochemical and theoretical studies. *J Mol Struct*. 2021;1225:129257.
- [66] Preethi Kumari P, Shetty P, Rao SA. Electrochemical measurements for the corrosion inhibition of mild steel in 1 M hydrochloric acid by using an aromatic hydrazide derivative. *Arabian J Chem*. 2017;10(5):653–663.
- [67] Madani A, Sibous L, Hellal A, et al. Synthesis, density functional theory study, molecular dynamics simulation and anti-corrosion performance of two benzidine schiff bases. *J Mol Struct*. 2021;1235:130224.
- [68] Chafiq M, Chaouiki A, Lgaz H, et al. Synthesis and corrosion inhibition evaluation of a new schiff base hydrazone for mild steel corrosion in HCl medium: electrochemical, DFT, and molecular dynamics simulations studies. 2019;34(12):1283–1314.
- [69] Salah M, Lahcène L, Omar A, et al. Study of corrosion inhibition of C38 steel in 1 M HCl solution by polyethyleneiminemethylene phosphonic acid. *Int J Ind Chem*. 2017; 8(3):263–272.
- [70] Li TL, Lu WC. Application of koopmans' theorem for density functional theory to full Valence-Band photoemission spectroscopy modeling. *Spectrochim Acta A Mol Biomol Spectrosc*. 2015;149:434–440.
- [71] Gritsenko O. V. Koopmans' theorem and its density-functional-theory analog assessed in evaluation of the red shift of vertical ionization potential upon complexation. *Chem Phys Lett*. 2018;691:178–180.
- [72] Mathiyalagan A, Manimaran K, Muthu K, et al. Density functional theory study on the electronic structures and spectral properties of 3,5-dimethylanisole dye sensitizer for solar cell applications. *Results Chem*. 2021;3:100164.
- [73] Hossen J, Pal TK, Hasan T. Theoretical investigations on the antioxidant potential of 2,4,5-Trihydroxybutyrophenone in different solvents: a DFT approach. *Results Chem*. 2022;4:100515.
- [74] Tüzün B, Bhawsar J. Quantum chemical study of thiazole derivatives as corrosion inhibitors based on density functional theory. *Arabian J Chem*. 2021;14(2):102927.
- [75] Hassan DA, Sultan HA, Al-Asadi RH, et al. DFT calculation and nonlinear optical properties of (E)-(2)-((8-Hydroxyquinolin-5yl)diazenyl)-5-sulfamoylphenyl)mercury(II) chloride. *Physica B Condens Matter*. 2022;639:413908.
- [76] Alamiery AA. Anticorrosion effect of thiosemicarbazide derivative on mild steel in 1 M hydrochloric acid and 0.5 M sulfuric acid: gravimetric and theoretical studies. *Mater Sci Energy Technol*. 2021;4:263–273.
- [77] Alamiery A. Corrosion inhibition effect of 2-N-phenylamino-5-(3-phenyl-3-oxo-1-propyl)-1,3,4-oxadiazole on mild steel in 1 M hydrochloric acid medium: insight from gravimetric and DFT investigations. *Mater Sci Energy Technol*. 2021;4:398–406.
- [78] Deng S, Li X, Du G. Two ditetrazole derivatives as effective inhibitors for the corrosion of steel in CH₃COOH solution. *J Mater Res Technol*. 2019;8(1):1389–1399.
- [79] Akalezi CO, Maduabuchi AC, Enenebeaku CK, et al. Experimental and DFT evaluation of adsorption and inhibitive properties of *Moringa oliefera* extract on mild steel corrosion in acidic media. *Arabian J Chem*. 2020;13(12):9270–9282.
- [80] Cheng Z, Yang B, Chen Q, et al. Characteristics and difference of oxidation and coagulation mechanisms for the removal of organic compounds by quantum parameter analysis. *Chem Eng J*. 2018;332:351–360.
- [81] Al-Qurashi OS, Wazzan N. Molecular and periodic DFT calculations of the corrosion protection of Fe(1 1 0) by individual components of aerva lanata flower as a green corrosion inhibitor. *J Saudi Chem Soc*. 2022;26(6):101566.

- [82] Gerrits N, Smeets EWF, Vuckovic S, et al. Density functional theory for molecule–metal surface reactions: when does the generalized gradient approximation get it right, and what to do if it does not. *J. Phys. Chem. Lett.* 2020;11(24):10552–10560.
- [83] Bahamon D, Khalil M, Belabbes A, et al. A DFT study of the adsorption energy and electronic interactions of the SO₂ molecule on a CoP hydrotreating catalyst. *RSC Adv.* 2021;11(5):2947–2957.
- [84] Experimental and theoretical evaluation of quercetin as a novel and eco-friendly corrosion inhibitor for C38 steel in hydrochloric medium | Abstract <https://www.der-pharmachemica.com/abstract/experimental-and-theoretical-evaluation-of-quercetin-as-a-novel-and-ecofriendly-corrosion-inhibitor-for-c38-steel-in-hyd-3973.html>. (accessed Nov 1, 2022).
- [85] Afia L, Lgaz H, Zougagh M, et al. Kaempferol as a corrosion inhibitor on mild steel in HCl. *App J Envi Engineering Sci.* 2016;2(2):42–55. 2.
- [86] Yin C, Kong M, Zhang J, et al. Influence of hydroxyl groups on the inhibitive corrosion of gemini surfactant for carbon steel. *ACS Omega.* 2020;5(6):2620–2629.
- [87] Guo L, Ren X, Zhou Y, et al. Theoretical evaluation of the corrosion inhibition performance of 1,3-Thiazole and its amino derivatives. *Arabian J Chem.* 2017;10(1): 121–130.
- [88] Haldhar R, Prasad D, Kamboj D, et al. Corrosion inhibition, surface adsorption and computational studies of *Momordica charantia* extract: a sustainable and green approach. *SN Appl. Sci.* 2021;3(1):1–13.